Linear viscoelastic model for elongational viscosity by control theory

Tommi Borg[1]

TomCoat Oy, Koskisenkuja 11, 62500 Evijärvi, Finland

Esko J. Pääkkönen

Tampere University of Technology, Laboratory of Plastics and Elastomer Technology, P.O. Box 589, 33101 Tampere, Finland

Flows involving different types of chain branches have been modelled as functions of the uniaxial elongation using the recently generated constitutive model and molecular dynamics for linear viscoelasticity of polymers. Previously control theory was applied to model the relationship between the relaxation modulus, dynamic and shear viscosity, transient flow effects, power law and Cox-Merz rule related to the molecular weight distribution (MWD) by melt calibration. Temperature dependences and dimensions of statistical chain tubes were also modelled. The present study investigated the elongational viscosity.

We introduced earlier the rheologically effective distribution (RED), which relates very accurately and linearly to the viscoelastic properties. The newly introduced effective strain hardening distribution (RED_H) is related to long-chain branching. This RED_H is converted to real long-chain branching distribution (LCBD) by melt calibration and a simple relation formula. The presented procedure is very effective at characterizing long-chain branches, and also provides information on their structure and distribution. Accurate simulations of the elongational viscosities of low-density polyethylene, linear low-density polyethylene and polypropylene, and new types of MWDs are presented. Models are presented for strain hardening that includes the monotonic increase and overshoot effects. Since the correct behaviour at large Hencky strains is still unclear, these theoretical models may aid further research and measurements.

Keywords: Elongational viscosity; Polydispersity; Control theory; Melt calibration; Long-chain branching

1. Introduction

This paper forms part of a series of papers on the use of control theory to model the viscoelastic properties of polymers. We first present a formula for

[1] To whom correspondence should be addressed.

uniaxial elongational viscosity without strain hardening, which is derived in a similar way to that used in previous studies, by starting from control theory. The next step involves including the effective strain-hardening distribution, which in many cases is related to long-chain branching. Some accurate simulation results related to elongation or extension are also presented.

It is beyond the scope of this article to provide a complete summary of all the group studies of elongational viscosity; more information on this is available in the historical reviews by Petrie[1] (for the last 100 years) and Mackley[2] (for the last 40 years). In recent decades measurements have made by Meissner and Hostettler,[3] Laun and Schuch,[4] Münstedt[5], Münstedt et. al. [6, 7] Sentmanat,[8] Hassager et al.[9], Aho et al.[10] and van Ruymbeke et. al..[11]

Fewer studies have modelled the elongational viscosity, among them being Wagner,[12, 13] Rolón-Garrido and Wagner, [14] Rolón-Garrido et. al.[15] with a generalization of the theory of Doi and Edwards,[16 , 17] Laun[18] on memory function, Rauschenberger and Laun[19] on recursive model, McLeish and Larson[20] and Inkson et al.[21] on "pom-pom" constitutive equations, Likhtman and Graham[22] on the Roli-poly model, Auhl et. al.[23] on the volume of tube and van Ruymbeke et. al. [24] by Mixing law and tube pressure.

We have previously published separate studies for different types of viscoelastic flows as relaxation modulus,[25] dynamic[26] and shear viscosity[27] related to the rheologically effective distribution (RED) and further molecular weight distribution (MWD). Temperature dependences and dimensions of statistical chain tubes were also modelled.[28] These papers explain more background for the used control theory, chain dynamics and developments of formulas.

Among other this study explains why dynamic frequency sweep measurements with oscillation rheometer with presence of possible amount of LCBs are preferred to carry out at constant strain controlled mode instead of widely used stress controlled mode.

The short review of the principle

General principle of control theory and models for elementary viscoelasticity are reviewed shortly. The modern control theory is used in many modern technologies as digital computers, aircrafts and process industry. As

control theory itself is mathematically well accepted principle over hundred years, procedure creates also to the target formulas linear model.

We excite the system with a small stress induced by a small pulsed strain that is applied at time t_0. Pulse response $y(t)$ is obtained from impulse response $h(t)$ and by sampling the active molecules in distribution $w(t)$ between some time interval:

$$y(t) = \int_{-\infty}^{t} w(\tau)h(t-\tau)\mathrm{d}\tau \qquad (1)$$

This equation is a familiar linear formula used in control theory, which is known as a novel principle to adjust and rule by one variable or function in a closed system and now in our case for rheologically effective distribution (RED) or $w(t)$ related to the MWD. This convolution integral differs from respective Maxwell type and Mixing laws as the functional Eq. (1) has no relaxation time procedures or variables at different scales. Thus there are fundamental differences in relaxation times λ and their discrete spectra are artificial, whereas continuous distribution RED $w(t)$ is a true function in the form of statistical distribution for viscoelastic effects and later related to the MWD.

Pulse response $y(\log t) = \log\frac{G(t)}{G_0}$ is a normalized relaxation modulus with a maximum value of zero on the logarithmic scale at t_0. The value for zero relaxation modulus $G_0 = G(t_0)$ is obtained by fitting $G(t)$ to experimental measurements. We then obtain the complete relaxation formula in the case where a small and constant strain is induced:

$$log\,\frac{G(t)}{G_0} = -P\int_{-\infty}^{log\,t} w(log\,\tau)(log\,t - log\,\tau)d\,log\,\tau, \qquad (2)$$

where impulse response $\log t - \log\tau = \log\frac{t}{\tau}$ and value for elastic constant P is obtained by feedback procedure of control theory. Presented Eq. (2) models accurately relaxation phenomena although viscous component and constant P" is not yet included as is discussed in more detailed explanation for relaxation modulus in Part I.[25]

Originally, we applied formula for modelling viscoelastic flows to get out computed MWD as we did in Part II.[26] The power of control theory is the fact that it reduces the need for using variables as we did in the Parts I–IV. [25–28]

During studies this same power was used to develop at first accurate viscoelastic fits for different flows and after that were found relations to the other microstructures as statistical tube dimensions discussed in Part IV. Thus our

development processes were done on the contrary as by earlier studies.[12–24] This unusual procedure guarantees accurate, simple but consistency model with physics for these complicated phenomena and flows. In other words we can go by step by step downwards for more detailed and complicated microstructures and still keeping the consistency of the model. The strength is the fact that polymer chain structure complexity is not limitation for good semi-empirical viscosity models and more challenge is coming from studying chain microstructure.

Already is published over sixty different new equations for different flows without using artificial relaxation time schema. As principle starts on a clean table and on new standpoint in rheology, developments cannot be evaluated by such as Occam's razor principle. Actually only few material dependent constants are used.

Until very recently was found that rheologically effective distribution (RED), which relates very accurately and linearly to the viscoelastic properties, is actually melt chromatogram as in liquid chromatography methods eluent, elution curve or elugram.

Model Development

Elongational viscosity $\tilde{\eta}_E^+(t)$ without strain hardening effect

We can directly write the formula in the start-up for uniaxial elongational viscosity $\tilde{\eta}_{\mathrm{E}}^{+}(t)$ using control theory in a similar way to previous work on the relaxation modulus and the dynamic and shear viscosities. The strain hardening effects coming from long-chain branches (LCBs) or similar structures are not yet included in to the elongational viscosity $\tilde{\eta}_E^+(t)$. As previously for the case in the start-up of shear viscosity being a function of shear and elongation, we have to use our new time–rate separability basis (which is new to rheology) when deriving functions for the parallel-resistor analogy[27]. Now the elongation is again a function of one rate variable, $\dot{\varepsilon}$, and hence we do not need to start from steady-state elongational viscosity $\eta(\dot{\varepsilon}) \equiv \frac{\sigma}{\dot{\varepsilon}}$—which is a function of constant Hencky strain rate $\dot{\varepsilon} = \frac{\mathrm{d}\ln\left(L/L_0\right)}{\mathrm{d}t}$ and constant tensile stress σ. Moreover, the steady-state elongational viscosity or "Trouton viscosity" is difficult to measure.

We use an alternative strategy to get elongational viscosity by imposing net tensile stress σ_{E} monitoring as a function of time. At first we model $\eta_{\mathrm{E}}^{+}(t)$ without any strain-hardening effects or influences of LCBs.

Thus, we write a characteristic formula directly for elongational viscosity $\tilde{\eta}_{\mathrm{E}}^{+}(t)$, where the tilde mark over the "η" indicates that the strain-hardening effect is not yet included:

$$\log\frac{\tilde{\eta}_{\mathrm{E}}^{+}(t)}{\tilde{\eta}_{0}^{+}} = -\log\frac{t}{t_c}\int_{-\infty}^{\log t}(Pw(\log\tau) + P'')\, d\log\tau \qquad (3)$$

where $\tilde{\eta}_{0}^{+}$ is the elongational viscosity at characteristic time t_c= 1/s similar way as earlier. We developed the formula similar way starting from control theory as for characteristic relaxation modulus $G_c(t)$ by Eq. (13),[25] characteristic complex viscosity η_c^* by Eq. (7)[26] and characteristic shear viscosity η by Eq. (1).[27] The rheologically effective distribution (RED) $w(\log t)$ relates not only to orientated but also stretched chains that lose their entanglements. RED function $w(t)$ can be regarded as respective chromatogram or elugram distribution with liquid chromatography of GPC/SEC. This RED, presenting here as an elastic component, influences the polymer normally after $t > 0.001$ s during elongation. Since the possible measurement range starts after $t > 0.01$ s, we do not need to use the $w''(\log t)$ component of the RED" distribution including viscoelastic effects, since it is always at normalized value $w'' = 1$ in these measurement ranges and hence can be simplified to $P''w''(\log t) = P''$. In most cases $P > 0$, but always $P'' < 0$.

A simple relation can be written for the melt calibration, $M(t)$, as a function of time, where the value of *Mf* is *M* at $t_1 = 1/s$:

$$M = Mf\left(\frac{t_1}{t}\right)^{\frac{1}{Hf}} \qquad (4)$$

This formula can be used to convert MWD $w(\log M)$ into RED $w(\log t)$ or $w(\log t) = w(\log M)$. Melt calibration has close similarities with the widely used linear broad-standard calibration with SEC, which approach requires a broad standard of known number-average M_n and weight-average M_w molecular weights. The use of different *Mf* and *Hf* values allows the REDs to be converted into their respectively MWDs, where *Mf* sets the absolute molecular weight and *Hf* sets the polydispersity value.

The analytical formula for viscosity $\tilde{\eta}_{\mathrm{E}}^{+}(\mathrm{t})$ can be written by applying a procedure similar to that used in our previous studies, but this was not required for the present study.

Strain hardening with a monotonically increasing effect

Elongational viscosity $\eta_{\mathrm{E}}^{+}(t)$ includes basic strain-hardening component originally $w_{\mathrm{H}}(\log \varepsilon)$ as a function of time *t* and elongation rate $\dot{\varepsilon}$ or effective strain-hardening distribution $w_{\mathrm{H}}(\log t, \dot{\varepsilon})$, where $t = {}^{\varepsilon}/_{\dot{\varepsilon}}$ with monotonically increasing behaviour, at least in the absence of the overshoot effect, as has been done in most other simulation models.

Long-chain branches (LCBs) and high-molecular-weight (HMW) end fractions impact strain-hardening effects on the initial elongation in elongation experiments. The origin of this additional response is the oriented and taut tied stretched chains between entanglements that did not have time to disentangle and relax. The longest chains are the first to exhibit this taut tied characteristic, and strong strain hardening begins to occur since they have no more free loops anywhere. Finally the flow becomes non-homogeneous on a micro or even a semi-micro scale, which accelerates the breakdown of elongation experiments.

Since hardening is related to the length of chains, LCBs and HMW end fractions, we set the respective hardening and rheologically effective distribution $\mathrm{RED_H}$ or $w_{\mathrm{H}}(log\ t, \dot{\varepsilon})$ (note that we are using the "H" subscript, even though the origin can also be other than LCBs or HMW end fractions). The strain-hardening effect is adjusted by the value of P_{H}. Now we can write the complete formula for start-up of elongational viscosity $\eta_{E}^{+}(t)$ as

$$\log \frac{\eta_{E}^{+}(t,\dot{\varepsilon})}{\eta_{0}^{+}} = -\log \frac{t}{t_c} \int_{-\infty}^{\log t} \left(Pw(\log \tau) + P'' + P_H(\dot{\varepsilon})\, w_H(\log \tau, \dot{\varepsilon}) \right) d \log \tau \quad (5)$$

For developing RED $w_H(\log t, \dot{\varepsilon})_{\mathrm{H}}$ we use its own $\mathrm{RED_H}$ according to Eq. (4) with its own *Mf* and *Hf* factors, since this rheological behaviour is totally different.

From the standpoint of molecular dynamics and the tube model described previously,[28] we obtain that statistical unit segment length L_{s} increases and diameter D_{s} decrease relatively for a unit backbone during elongation. Elasticity function $P' = k' \frac{D_{\mathrm{s}}}{L_{\mathrm{s}}}$ and especially P_{H} decrease in a similar way in Eq. (5) giving less strain hardening effect.

For the used elongation rates, with $\dot{\varepsilon}$ <1/s, meaningful differences to $\eta_E^+(t)$ values are not observed at the beginning (i.e., $t < 0.1$ s), but the amount of strain hardening depends on the used rate described by strain-hardening coefficient $\chi(t, \dot{\varepsilon})$. [29, 30] They discuss the molecular structure, referring to long-chain branching. But no simulation model is presented for absolute measured values of $\chi(t, \dot{\varepsilon})$, thus we have to develop a simple model to perform modelling and obtain simulation results. The strain-hardening effect, $P_H(\dot{\varepsilon})$, is linearly related to strain-hardening coefficient $\chi(t, \dot{\varepsilon})$. Normalized distributions $w(\log t)$ and $w(t, \dot{\varepsilon})$ and strain hardening effects during different strain rates are shown in Fig. 1.

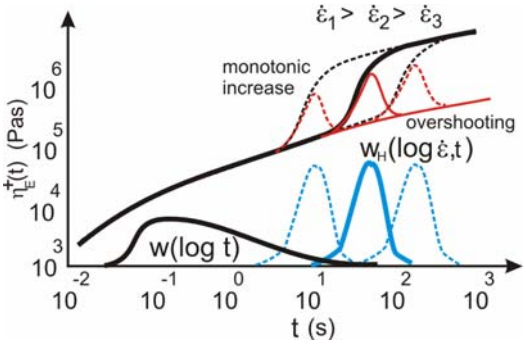

Figure 1. Elongational viscosity $\eta_E^+(t)$ with LCBs giving strain hardening, and a schematic model for converting REDs and REDHs into the respective MWDs. RED_Hs are scaled with their effectiveness by $P_H(\dot{\varepsilon})$ values or $P_H(\dot{\varepsilon})$ $w_H(\log t, \dot{\varepsilon})$, where $\varepsilon = \dot{\varepsilon}t$ at different elongation rates according to Eq. (5) for a monotonic increase and Eq. (6) for the overshoot strain-hardening effects.

The above-described procedure for simulations is rather insensitive to the actual form of the used MWD, which make it possible to use MWD data copied from the literature or to use nominal distributions. The results are much more sensitive to the actual form of the LCBD and $w_H(log\ t, \dot{\varepsilon})$.

Strain-hardening component $w_H(log\ t, \dot{\varepsilon})$ with the overshoot property

The elongational viscosity at large strains has been studied less, as has strain-hardening viscosity. Rasmussen et al.[31] measured the viscosity at large Hencky strains of up to 6–7 for low-density polyethylene (LDPE) as shown in Fig. 3 and linear low-density polyethylene (LLDPE). They observed that LLDPE behaves as shown in Fig. 4 and according to Eq. (5), whereas LDPE exhibits a viscosity overshoot effect that appears as a bump. We thus rewrite Eq. (5) for the overshoot-type strain hardening as follows:

$$\log\frac{\eta_E^+(t)}{\eta_0^+} = -\log\frac{t}{t_c}\left(\int_{-\infty}^{\log t}(Pw(\log\tau)+P'')d\log\tau\ + P_H(\dot{\varepsilon})w_H(\log\tau,\dot{\varepsilon})\right) (6)$$

The form of the left side of strain-hardening distribution $w_H(\log t,\dot{\varepsilon})$ is similar to that at the beginning of strain hardening from Eq. (5) or (6). However, the final form of the subsequent strain hardening remains unclear.

Burghelea et al.[32] very recently argued that the overshoot phenomena are not real rheological features but rather merely represent artefacts resulting from the strong geometric non-uniformity of the sample at high Hencky strains. If it does exist, strain hardening could be described as a mixture of Eqs. (5) and (6), but we are unable to derive these combined formulas since there are insufficient data available at high Hencky strains. Fortunately this has little effect on the obtained left side of strain-hardening distribution RED_H or the right side of LCBD.

Effective strain-hardening distribution RED_H from elongational viscosity measurements

We extract strain-hardening distribution RED_H from Eq. (5) using a procedure similar to that described for the relaxation modulus[25] or shear viscosity[26]. We obtain $w_H(\log t,\dot{\varepsilon})$ by deriving as follows from the measured differences to $\eta_E^+(t)$ to accurately obtain the shape of the RED_H curve:

$$w_H(\log t,\dot{\varepsilon}) = -\frac{d}{d\log t}\frac{1}{P_H(\dot{\varepsilon})}\left(\frac{\ln\frac{\eta_E^+(t)}{\eta_0^+}}{ln\frac{t}{t_c}}+\int_{-\infty}^{\log t}(Pw(\log\tau)+P'')\,d\log\tau\right) (7)$$

Eq. (6) or a mixture of Eqs. (5) and (6) can be solved in a similar way to obtain RED_H, but this was not done in this study.

Long-chain branching distribution

Strain-hardening distribution RED_H is converted to direct relation of long-chain branching distribution (LCBD) by melt calibration with a simple relation formula. Real distributions for LCBDs have very rarely presented with MWD in literature.

A nuclear magnetic resonance method (NMR) is used to detect LCB, but is known that NMR can be used to detect side chain branches with up to 8 carbon atoms only.[33] Many alternative ways have been developed to obtain a single numerical value[34, 35, 36, 37, 38, 39] including by utilizing the Zimm–Stockmayer equation.[40] Several rheological methods are suitable for identifying LCB,[41, 42, 43, 44, 45, 46] such as van Gurp–Palmen[47, 48] and Cole–Cole[49] plots, flow activation energy,[50] thermorheology,[51] the dynamic modulus,[41] and relaxation times, but all suffer from the problem of not being able to convert the obtained results into absolute numerical values.

Applying a stochastic approach to topological LCBD models has yielded the multidimensional distributed molecular properties (e.g., joint MW–LCB distribution) with the number of long chain branches. [52, 53, 54]

We employ a different procedure using a more realistic one-dimensional LCBD with the total number of inner backbones. In Fig. 2a on the left is shown used terminology[55] for the primary chain as backbone, directly linked chains are free arms and next connected chains are inner backbone segments. Of course this LCBD in Fig 2b can be fractionalized later on to bivariate MW–LCB distribution if needed.[54] Main distribution $w_{MAIN}(M)$ can be detected rheologically[26] or by GPC/SEC, which is used mainly for this study and known also insensitive to detect LCBs. For showing final results we use sum of RED or MWD distributions to get normalized sum value one as follows: $\int w_{MAIN} + \int w_{LCB} = 1$.

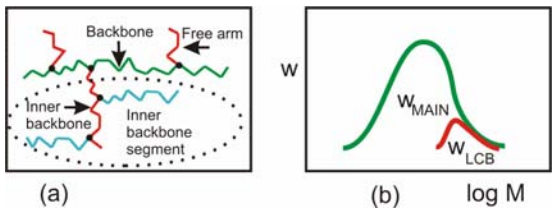

Figure 2. Schematic diagram of detecting LCBD $w_{LCB}(M)$.

a. Molecule chain has backbone, free arms and inner backbone segments.

b. From GPC/SEC or by using narrow dynamic viscoelastic data range to get normalized MWD or $w_{MAIN}(M)$. From strain-hardening distribution $w_H(\log t, \dot{\varepsilon})$ and own *Mf* and *Hf* values for melt calibration we get absolute LCBD or $w_{LCB}(M)$ distribution.

LCB distribution as a function of M or $w_H(M) = w_H(\log t, \dot{\varepsilon})$, where $\dot{\varepsilon} = 1/\mathrm{s}$ used in this study, is gained by the right selection for Eq. (4) by their own values *Mf* and *Hf* for melt calibration similar way as are done with calibration curve and GPC/SEC procedures. As constants P and P_H set effects for

viscoelastic properties and they are inside log function, we get simple formula for strain-hardening coefficient $\chi(\dot{\varepsilon})$ = log ($P_H(\dot{\varepsilon})/P$) as both constants in Eq. (5) are inside logarithm. The influence of right size for final LCB distribution $w_{LCB}(M)$ by using relation $1/\chi$ of normalized MWD and LCBD as follows

$$w_{LCB}(M) = \frac{1}{M_b}\log\left(\frac{P_H}{P}\right)w_H(M), \quad (8)$$

where M_b is molar mass m of a backbone element, for PE M_b = 14mol/g. In principle LCBD can be outside of MWD even though measured by GPC/SEC, as these methods do not detect LCBs. Thus we get absolute LCBD or $w_{LCB}(M)$ by using different structural value *Mf* and conversion factor *Hf* for conversion from RED_H.

We can renew the formula for the LCB frequency—expressed as the number of long chain branches per 1,000 carbon atoms as presented in previous studies[39, 45]—using the above results for LCBD as follows:

$$LCB/_{1000\ C} = 1000M_b\sum\frac{w_{LCB}(M_i)}{M_i} \quad (9)$$

where w_{LCB} is the weight fraction of LCBD, M_i is the MW of each fraction, and M_b is the molar mass of a backbone element [M_b = 14 for polyethylene (PE)]. Complete weight fraction w_i of the MWD and the average number of branches per molecule were originally used in the formula.[39] However, now this value consists not only of branches on the backbone but also of inner backbones, as shown in Fig 2a. A major disadvantage of these types of formulas is that the average MW of backbones (and now branches) strongly influence the obtained values.

Experimental Section

Test polymers and constants

Strain hardening that occurs during elongation of a branched structure was modelled. The measured elongational viscosity was simulated as a function of different elongation rates using control theory, including for higher Hencky strains that have not yet been measured. The results are compared here with those that have been observed, and we also discuss more generally used principles,

hypotheses, and structures of models and formulas. The measurements made by Stadler et al. [30] and Münstedt et al.[56] were simulated.

The MWD was measured carried by a high-temperature GPC coupled with a multiangle light-scattering apparatus (MALLS). MWD for LDPE come from RheoPower Database. As we know, GPC is not sensitive to detect LCBs.

Elongational viscosity simulations were performed by executing a characteristic model of control theory on a standard PC with the commercial RheoPower software package using the RheoDeveloper program with experimental elongation moduli. We did not need to use the more sensitive RheoAnalyzer program for MWDs, since their effects on the rheological properties are less than those of LCBDs in this application. Our description of results starts by using functional formulas of Eq. (3) giving accurate real fits with measurements by adjusting RED_H, then is shown and discussed different strategies for modelling elongational viscosity at high Hencky strains. Along calculation is some words of LCB average chain length and distribution and branching intensity. One bivariate RED- RED_H distribution chart as a function of time and rate is shown and finally MW-LCB distribution results converted to two apparent MWD charts.

Procedure

The elongational viscosity was modelled first without and then with strain hardening. Since the presented formulas are new, and hence the values of constants are unknown, we explain the step-by-step best-fit routine and by Fig. 3 based on the measurements and our model starting from control theory. We did not use Eq. (7) to detect $w_H(\log t, \dot{\varepsilon})$ in this study, since we fitted our curves with previously published measured data. We obtained that manually copied data to derive by Eq. (7) was sensitive to errors. The elongational viscosity is first developed without the strain-hardening effect, which involves the following steps:

1. Draw a known MWD in the RheoDeveloper program and save it in a database. Set *Mf* and *Hf* constants as a-priori information using values found previously for the complex viscosity.
2. Set first test *P'*, *P"* and zero $\tilde{\eta}_0^+$ values for the polymer sample, and compute and compare them with measured elongation values.

Adjust the values so that the simulation result on the output chart is as close as possible to images imported from measured data.

3. Alter the *Mf* and *Hf* values and repeat step 2.
4. Modify and alter a little-known MWD to see if errors between the modeled and measured results increase so as to check if the used MWD is acceptable.
5. Test different types of polymer samples in order to ascertain the correct values for constants. Repeat the above steps as many times as necessary to obtain satisfactory results, at which point you can proceed to the next level.

The following LCBD iteration routine involves the strain-hardening function and distribution:

1. Set separate *Mf* and *MwR* values for hardening distribution $\mathrm{RED}_{\mathrm{H}}$ $w_{\mathrm{H}}(\log t, \dot{\varepsilon})$ with strain-hardening constant $P_{\mathrm{H}} > 0$.
2. Obtain some elongation rates $\dot{\varepsilon}$ and compare them with measurements. If necessary, select new *Mf* and *Hf* constants for $w_{\mathrm{H}}(\log t, \dot{\varepsilon})$.
3. Check the values with different polymers and attempt the obtain the best fit by using different *Mf*, *Hf*, $\eta_{\mathrm{E}}^{+}(t)$, $P_{\mathrm{H}}(\dot{\varepsilon})$ and $\dot{\varepsilon}$ values.
4. You can try to get better fit by drawing manually hardening distribution RED $w_{\mathrm{H}}(\log t, \dot{\varepsilon})$.
5. Save the final results in ASCII format in log-0.2 steps on a wide timescale and on the strain rate matrix.

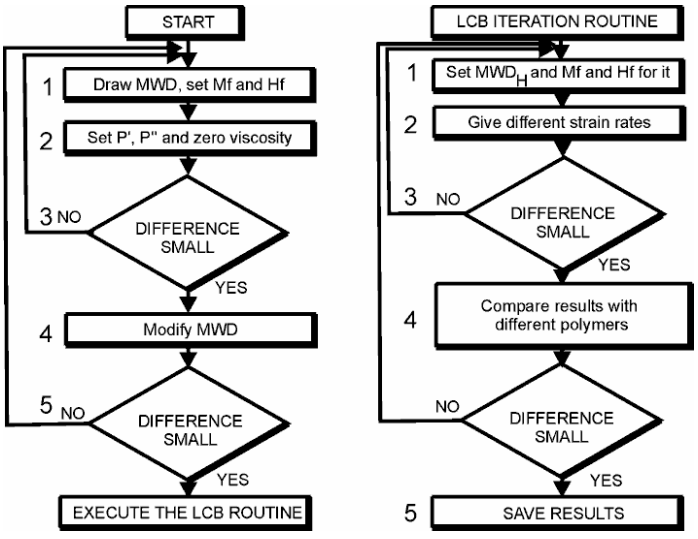

Figure 3. Flowchart of the simulation procedure.

The data can be processed further on a spreadsheet such as Excel® so as to combine MWD and LCBD. Measured data can be joined in CAD such as using the CorelDraw® program with the modelled and simulated results.

Results and Discussion

Used main characteristics

A polymer structure is modelled by the values *P*', *P*" and zero viscosity η_0^+, polymer structural value *Mf* and conversion factor *Hf* between scales. The values of *P*' and *P*" obtained from the viscosity fitting procedure are listed in Table 1, and no ad hoc constants or values were used. A constant temperature of T = 150°C was used for LDPE and LLDPE, while T = 180°C was used for polypropylene (PP).

For the effective strain-hardening distribution LCBD we used constant value *Hf* = 0.6 to allow comparisons between different samples. The used *Mf* values might not be accurate, but it is within the correct range and of course its value differs at least for PP.

The main characteristics of the samples are listed in Table 1.

	LDPE	LLDPE	PP 2	CSTR-LDPE 1	CSTR-LDPE 2
Mw[a]	213,000	102,000	574,000	4,167,000	2,271,000
MwR[a]	12.9	3.2	9.3	21.4	14.3
Mf[b]	70,000	30,000	200,000	70,000	70,000
Hf[b]	2.05	2.05	4	2.05	2.05
η_0^+[c]	4.6	4.68	4.1	4.87	4.18
P'[d]	0.42	0.65	0.56	0.22	0.51
P"[d]	–0.7	–0.7	–0.8	–0.68	–0.68
P_H[e]	2.6	2	2.6	4	3.4
Mw LCBD[f]	10,640,000	9,670,000	7,150,000	17,030,000	9,670,000
MwR LCBD[f]	5.3	2.7	1.4	6.5	2.7
Mf[g]	4,000,000	4,000,000	4,000,000	40,000,000	40,000,000
X	1.8	1.1	1.5	2.9	1.9
LCB/1000 *C*[h]	0.022	0.012	0.034	0.001	0.002

Table 1. Main characteristics of all investigated samples and computations.

[a]The used *Mw* (g/mol) and *MwR* values may differ slightly from those measured using GPC/SEC.

[b]Polymer structural value *Mf* (g/mol) and conversion factor between scale *Hf*.

[c]Elongational viscosity (Pas) at t = 1/s.

[d]Obtained elasticity *P*' and *P*" viscosity values.

[e]Strain-hardening constant P_H at rate $\dot{\varepsilon}$ =1/s.

[f]*Mw* (g/mol) and *MwR* values obtained for the effective strain-hardening distribution.

[g]Polymer structural value *Mf* (g/mol) for strain-hardening distribution, *Hf* = 0.6.

[h]Strain-hardening coefficient $\chi(\dot{\varepsilon})$ at rate $\dot{\varepsilon}$ =1/s.

[i]Long chain branching frequency per 1000 C carbon atoms.

Uniaxial elongational viscosity as a function $P_H(\dot{\varepsilon})$

We model uniaxial elongational viscosity according to measurements, but at a much higher Hencky strain (ε) compared to that obtained in practical measurements (this topic is discussed in Section 4). We first simulate a modern LDPE (Lupolen 1840 H) for well known and classical IUPAC A, as done previously our studies. The elongation viscosity results are shown in Fig. 4 and used RED_H functionals with $P_H(\dot{\varepsilon})$ in Fig. 5 according to Eq. (5).

We observe that simulation results accurately fit the measurements made by Münstedt et al..[56] Since the elongation software moduli of the RheoDeveloper program was still an experimental version, the output of the elongation viscosity was still in log-0.2 steps, which corresponds to the following elongation rates: 0.01/s, 0.016/s, 0.025/s, 0.04/s, 0.06/s, 0.1/s, 0.16/s, 0.25/s, 0.40/s, 0.6/s and 1/s. On the other hand, elongation rates of 0.01/s, 0.1/s and 1/s were used during measurements, whereas the data were for 0.002/s, 0.003/s, 0.03/s, 0.05/s and 0.5/s, which fall between the modelled elongation rates.

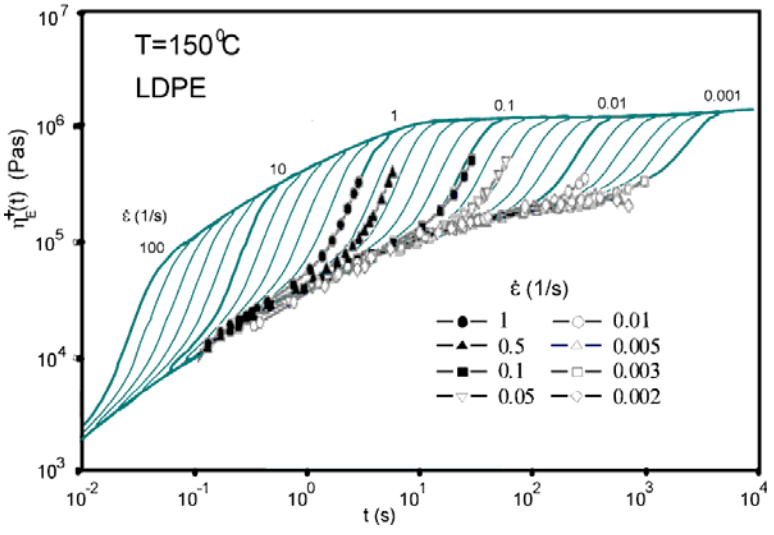

Figure 4. Modelled steady elongational viscosity $\eta_E^+(t)$ flow curves as functions of time for different elongation rates ($\dot{\varepsilon}$) from 0.001 to 100 s (lines), and data measured by Münstedt et al. for LDPE (symbols).[56] Modelled rates on decades (e.g., 10/s, 1/s and 0.1/s) are indicated by thicker lines.

As steady-state elongation viscosity is sometimes thought to run through a maximum as a function of elongation rate, we can simulate this by using smaller strain-hardening constants P_{H} at higher elongation rates. Used products for Fig. 4 this time variable $P_{\mathrm{H}}(\dot{\varepsilon})$ as a function of rate and effective strain-hardening distribution $\mathrm{RED}_{\mathrm{H}}$ or $P_{\mathrm{H}}(\dot{\varepsilon})$ $\mathrm{RED}_{\mathrm{H}}$ can be seen on Fig. 5. We have three important structures: the average LCB chain length and its distribution. Thirdly, the amount of LCB branches has no doubt a lot of effect.

We can obtain that $\mathrm{RED}_{\mathrm{H}}$s related to branches has much shorter and sharper effect on the elongation viscosity than RED related to the backbones of chains. The phenomenon indicates that longer chain lengths of LCBD have more influence as shorter ones behaving similar way as in melt calibration principle.

It is clear that the modelled curves accurately fit the measurements, with some differences being due to the use of different elongation rates during measurements and simulations, and at low rates ($\dot{\varepsilon}$ < 0.01/s) due to relaxation of taut tied chains.

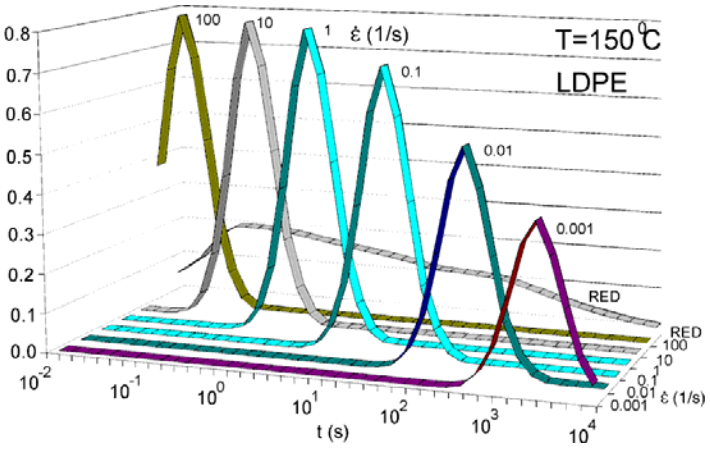

Figure 5. Used $P_{\mathrm{H}}(\dot{\varepsilon})$ $w_H(t,\dot{\varepsilon})$ products for generating Fig. 4 by product of $P_{\mathrm{H}}(\dot{\varepsilon})$ and effective strain-hardening distribution $\mathrm{RED}_{\mathrm{H}}$ or $w_H(t,\dot{\varepsilon})$ shown only on decade steps of $\dot{\varepsilon}$ for clarify. On the back is shown segment of used RED on time scale related to MWD.

Modelled elongational viscosity at high Hencky strains

We now try to understand the mechanism underlying the observed and measured strain-hardening effects and the accuracy of the extrapolations for high Hencky strains. Strain hardening, which occurs during film blowing or sheet foaming, is a useful and wanted feature in many practical plastic manufacturing processes. This property influences film casting and coating processes and it also gives the final end product a kind of self-healing mechanism. On the other hand it has drawbacks with LCBs in that it represents a source of strong and long-duration shrinkage that can cause the end products to warp. Strain hardening has also been exploited as a useful feature for heat-shrinkable sleeves, as described in the US patent by Borg.[57]

As discussed above, strain hardening is sensitive to LCBs and HMW end fractions, which we attribute to long taut tied stretched chains between entanglements not having sufficient time to disentangle and relax, causing inhomogeneity on a micro or even a semi-micro scale due to smaller chain bundles combining. Burghelea et al.[32] measured a significant difference between the normally used integral form for viscosity and the locally measured elongational viscosity. They discussed geometric non-uniformity and its relation to the stress maximum. Although we are studying macromolecules here, the longest LCB can still have an oriented length of many microns, which can induce local inhomogeneity in smaller bundles of molecules that causes breakdown during elongation measurements. Fibrilar structure and morphology development of blends during and after elongational deformation were observed by Starý et al.[58]

The elongation experiment with the Hencky strain variable with a strongly diminishing cross-section differs from many other procedures, and the local inhomogeneity in macromolecular chains can rapid break down the elongation. On the other hand, large cross-sections produce inaccurate measurements. Elongation experiments are difficult to carry out at the laboratory scale, but they are very important for understanding the behaviour and structure of polymers. Steady macro-scale plastic manufacturing processes may achieve much higher Hencky strains, and thus it might be necessary to model the complete rate range and even strains outside achievable measurement ranges.

Measured and modelled elongational viscosities for LLDPE are shown in Fig. 6. The stresses are orders of magnitude less than for LDPE in Fig.4. This time we have used constant value for strain-hardening value P_H as the data of measurements at higher rates.

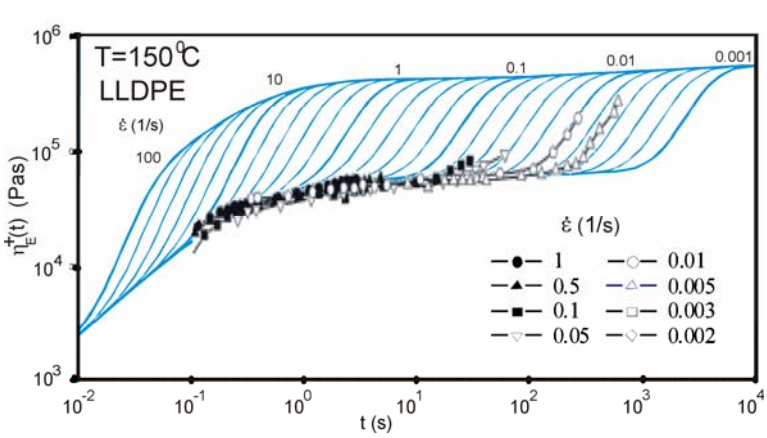

Figure 6. Measured and modelled elongational viscosities for LLDPE. The stresses are orders of magnitude less than for LDPE in Fig. 4.

Comparison of Figs. 4 and 6 reveals that strain hardening has a greater effect at higher elongation rates for LDPE and at lower elongation rates for LLDPE. Several possible mechanisms could underlie the strain hardening of LLDPE, including the presence of a few LCBs or components with high molar masses, which are not detectable by classical analytical methods, and phase separation in the molten state.[59] Strain hardening may peak at various times of elongation measurements, which has been studied recently by Stadler et al..[30] Since the underlying mechanism remains somewhat obscure, we did not try to model this feature but instead used the best fit with maximal strain hardening and the same level for all elongation rates.

The next puzzle is the possibility of overshoot during elongation. Rasmussen et al.[31] obtained an overshoot for LDPE Lupolen 1840 D, whereas Burghelea et al.[32] argued that this phenomenon does not exist. This discrepancy is why we present all of our simulation results as monotonically increasing without an overshoot effect in charts for visual clarity; moreover, although the amount of overshoot is not known, we still believe that some overshoot is present (as discussed above).

In summary, the present measurements accurately provided the left side of the effective hardening distribution RED_H or LCBD, where this procedure is

sensitive to the results. The level of strain hardening was obtained by fitting procedure.

Simulations of polymers with a high level of hardening

Polymers with a high level of hardening and LCB were simulated. For comparison we show a different chemical type of polymer in Fig. 7. The simulated data were the measurements of the highly branched PP made by Münstedt et al.[56] and used for all results for demonstration purposes constant strain-hardening P_H value, but uncertain results at higher elongations are dashed in the figure.

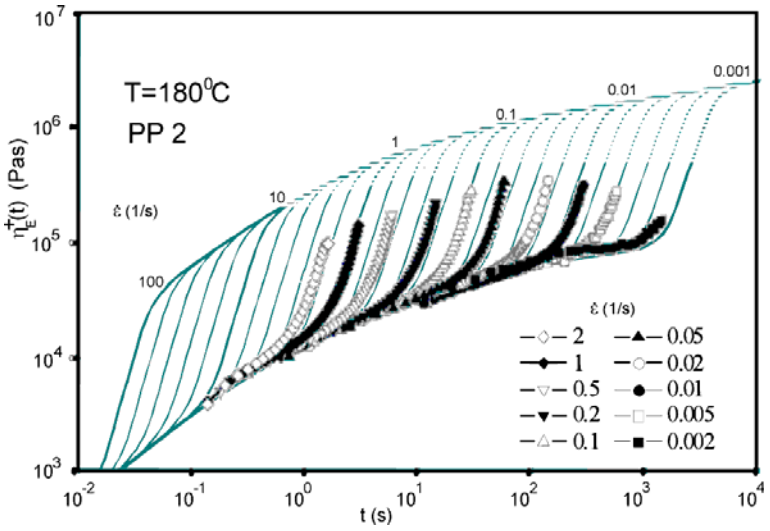

Figure 7. Simulated results using Eq. (5) for highly branched PP according to measurements by Münstedt et al.[56] (sample designated as PP 2 in that report). Strain hardening occurs over a wide range of elongation rates. Since the measurements do not show any overshoot, a large-strain approximation is used according to Eq. (5). We used constant strain-hardening P_H to simulate approximations in this case.

The last two presented simulations are of high-molecular-weight LDPEs known to have a very high LCB content: (1) including many LCBs polymerized at the laboratory scale in a continuously stirred tank reactor (CSTR) and (2) the polymer designated as CSTR-LDPE 1. The results are shown in Fig. 8. We did not know whether or not overshoot was present or the form of LCB distribution, which is why we used Eq. (5) without the overshoot effect in the monotonically increasing form for visual clarity (as discussed above). One novel interesting feature of this simulation was that its results were consistent with the measured strain-hardening spectrum for rates (i.e., $\dot{\varepsilon}$ values) of 0.1/s and 0.01/s, but not for rates of $\dot{\varepsilon}$=10/s and 0.001/s.

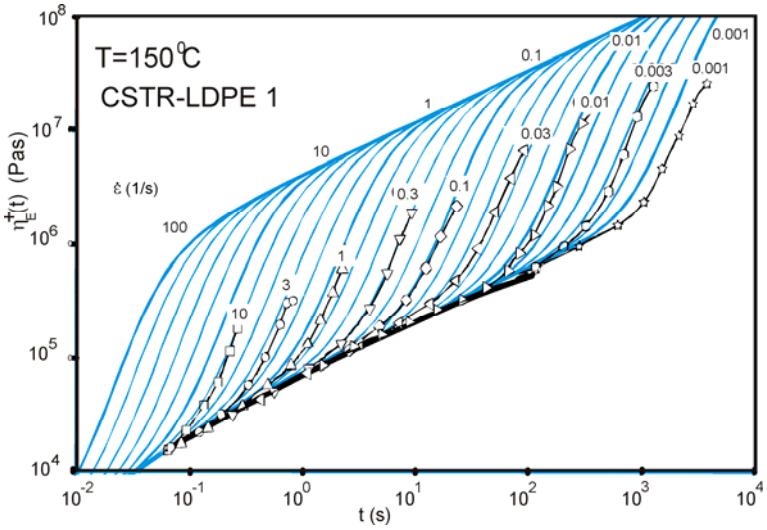

Figure 8. Simulated and measured spectra for CSTR-LDPE 1, with a high content of LCBs.

The results for another polymer, designated CSTR-LDPE 2 and which has fewer LCBs, are shown in Fig. 9. The simulation results for this polymer were consistent with the measured strain-hardening spectrum for all rates. Moreover, the hardening effect was not as strong as in Fig. 8.

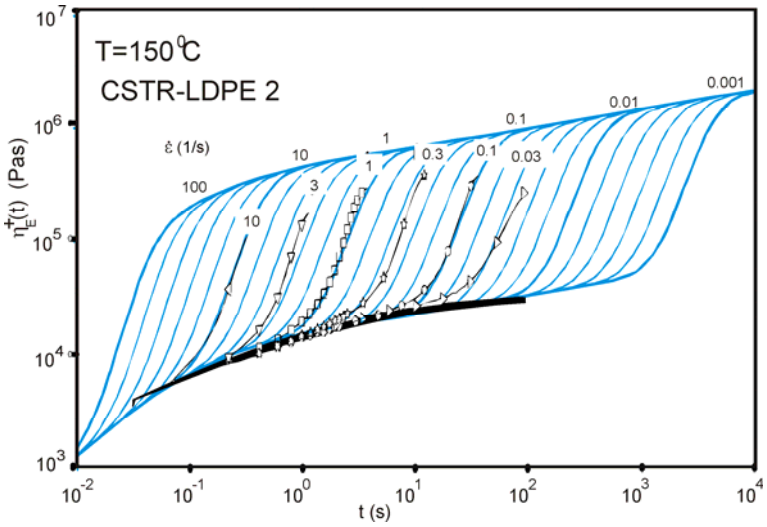

Figure 9. Simulated and measured spectra for CSTR-LDPE 2, with a lower content of LCBs.

Simulated MW-LCB distributions.

We generate long-chain branching distribution (LCBD) with MWD by melt calibration Eq. (4) and by relation formula Eq. (8). RED_Hs were obtained by a best-fit routine on a step-by-step basis based on the measurements and presented formulas. During the procedure it was found that the results were very sensitive even to the local forms of RED_Hs, which meant that we had to draw the final form

of the distribution curve manually in many cases. Since the shape of the LCB distribution is the same on a logarithmic scale as the original RED_{HS}, the results provide valuable information on polymer structure and the constituent LCBDs.

We selected for conversions by melt calibration for $w_H(\log t, \dot{\varepsilon})$, where $\dot{\varepsilon}$=1/s. We depicted in Fig. 5 accurate RED- RED_{HS} chart, now we present strain-hardening distributions converted by melt calibration Eq. (4) to LCBD $w_H(log\ M)$ on M scale.

The $w_H(\log t, \dot{\varepsilon})$ strain-hardening distributions are scaled by their strain-hardening constant P_H and respective main normalized MWDs in order to help readers to evaluate the final bimodal MWD distributions in Figs. 10 and 11. Fig. 10 presents the MWDs and LCBDs used for commercial LDPE, LLDPE and PP.

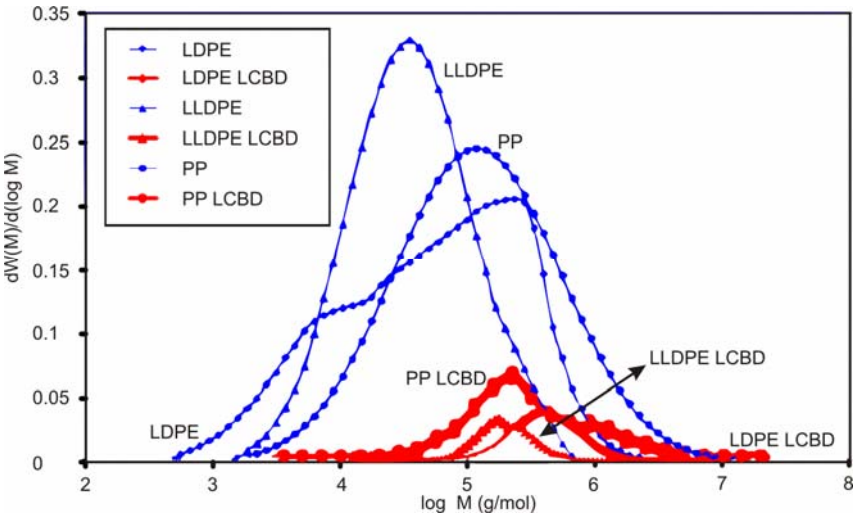

Figure 10. The used MWDs and LCBDs, obtained from effective strain-hardening distribution RED_H or $w_H(\log t, \dot{\varepsilon})$ by Eq. (8) for LDPE, LLDPE and PP simulations. Normalized MWD for LLDPE and PP were extracted from GPC/SEC measurements and LDPE from RheoPower database.

Fig. 11 depicts MWDs and LCBDs for LDPE formed at the laboratory scale and containing a large amount of LCBs. The figure shows similarities with data obtained by GPC/MALLS and the LCBs detected using our new method.

One interesting finding is that the PE polymer polydispersity of LCBDs follows the polydispersity of the main MWDs, and also the PP spectrum appears sharp.

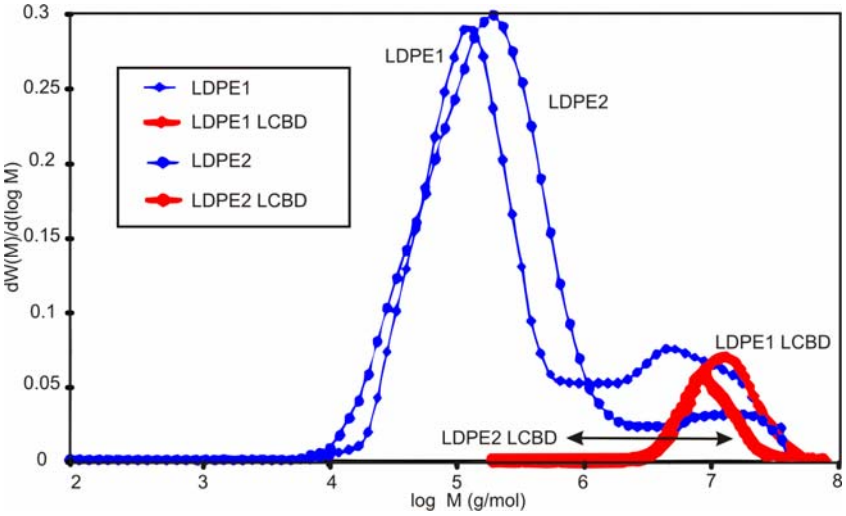

Figure 11. The used MWDs and LCBDs, obtained from effective strain-hardening distribution $\mathrm{RED}_{\mathrm{H}}$ or $w_{\mathrm{H}}(\log t, \dot{\varepsilon})$ by Eq. (8) for LDPE simulations. MWDs are from GPC/MALLS measurements. Best-fit procedures revealed similarities between LCBDs as observed previously.

Conclusions

We have presented models and simulations of the elongational viscosity. The obtained results indicate that the presented method is much more accurate at detecting LCBs and even LCBDs than any other known method. However, deeper studies involving more data must be performed in order to obtain the correct *Mf*, *Hf* and P_{H} values or even complete $P_{\mathrm{H}}(\dot{\varepsilon})$ function for the strain-hardening distribution, which gives surely information of the inner backbone segments. More research is also needed into the possibility of an overshoot effect and its underlying mechanism, but this is not essential for detecting LCBs because the present method is already able to detect about half of the complete LCBD. We notice that single value for long chain branching frequency per 1000 C carbon atoms (LCB/1000 C) is rather poor to describe branching although we had opportunity to use LCBD as source data for computations.

The demonstrated properties represent only a small proportion of the additional different applications for viscoelasticity and material analyses obtainable from control theory. In practical manufacturing applications, this elongation-based and (with LCBs) self-healing property is familiar, and it is expected that future developments in measuring instruments will allow this phenomenon to be fully described and analyzed.

The presented principles and multipurpose RheoPower software can be used to simulate viscoelastic properties and material structures by generating accurate linear relationships between them. Control theory avoids the need to obtain the true absolute values, although the differences between the obtained relative values must be accurate. This means that we can use not only shear or dynamic viscosities or respectively the moduli or the elongational viscosity, relaxation modulus or temperature, but also any (force-dependent) unit to obtain a linear relation. Thus, the property variable can be the shear rate, frequency, elongation rate, time, temperature or even, in principle, turns, rotations or revolutions per second.

Moreover, macromolecules typically exhibit some distribution-dependent behaviours, and thus the method is applicable to any material that is consistent with the property of polydispersity, such as a collection of particles of any size, objects or polymers that possess kinetic energy. Our novel melt calibration principle makes it possible to find the real weight or size relating to the viscoelasticity. The principle and software were originally developed for polymer simulations, but the presented curves indicate that the technique can also be flexibly applied in other rheological applications.

Used nomenclature:

P	Elastic constant
P''	Viscous constant
P_{H}	Maximal strain-hardening constant
$P_{\mathrm{H}}(\dot{\varepsilon})$	Strain-hardening variable
t_{c}	Characteristic time
ε	Hencky strain
$\dot{\varepsilon}$	Elongation rate
$\eta_0^+, \tilde{\eta}_0^+$	Elongational viscosity at characteristic time t_{c} = 1/s.
$\tilde{\eta}_{\mathrm{E}}^+(t)$	Elongational viscosity without strain hardening effect
$\eta_{\mathrm{E}}^+(t)$	Elongational viscosity including strain hardening effect
σ_E	Net tensile stress monitoring as a function of time
LCBD, $w_{\mathrm{LCB}}(M)$	Long-chain branching distribution
MWD, $w_{\mathrm{MAIN}}(M)$	Molecular weight distribution obtained by GPC/SEC
RED, $w(\log t)$	Rheologically effective distribution (elastic)
$w_{\mathrm{H}}(\log \varepsilon)$	Original strain-hardening component

RED_H, $w_H(\log t, \dot{\varepsilon})$	Effective strain-hardening distribution as a function of time and rate
$\chi(t, \dot{\varepsilon})$	Strain-hardening coefficient

References

1. Petrie CJS (2006) One hundred years of extensional flow, J Non-Newtonian Fluid Mech 137: 1–14
2. Mackley M (2010) Stretching polymer chains Rheol Acta 49: 443–458
3. Meissner J, Hostettler J (1994) A new elongational rheometer for polymer melts and other highly viscoelastic liquids, Rheol Acta 33: 1–21
4. Laun HM, Schuch H (1989) Transient elongational viscosities and drawability of polymer melts J Rheol 33:119–175
5. Münstedt H (1979) New universal extensional rheometer for polymer melts J Rheol 23: 421–436
6. Münstedt H, Kurzbeck S, Egersdörfer L (1998) Influence of molecular structure on rheological properties of polyethylenes Part II. Elongational behavior Rheol Acta 37: 21–29
7. Münstedt H, Steffl T, Malmberg A (2005) Correlation between rheological behaviour in uniaxial elongation and film blowing properties of various polyethylenes Rheol Acta 45: 14–22
8. Sentmanat M (2004) Miniature universal testing platform: from extensional melt rheology to solid-state deformation behaviour Rheol Acta 43: 657–669
9. Hassager O, Marin JMR, Yu K, Rasmussen HK (2010) Polymeric liquids in extension: fluid mechanics or rheometry? Rheol Acta 49: 543–554
10. Aho J, Rolón-Garrido VH, Syrjälä S, Wagner MH (2010) Measurement technique and data analysis of extensional viscosity for polymer melts by Sentmanat extensional rheometer (SER), Rheol Acta 49: 359–370
11. van Ruymbeke E, Muliawan EB, Hatzikiriakos SG, Watanabe T, Hirao A, Vlassopoulos D (2010) Viscoelasticity and extensional rheology of model Cayley-tree polymers of different generations, J Rheol 54: 643–662.
12. Wagner MH (1979) Zur Netzwerktheorie von Polymer-Schmelzen Rheol Acta 18: 33–50
13. Wagner MH, Kheirandish S, Stange J, Münstedt H (2006) Modeling elongational viscosity of blends of linear and long-chain branched polypropylenes, Rheol Acta 46: 211–221
14. Rolón-Garrido VH, Wagner M H (2007) The MSF model: relation of nonlinear parameters to molecular structure of long-chain branched polymer melts Rheol Acta 46: 583–593
15. Rolón-Garrido VH, Pivokonsky R, Filip P, Zatloukal M, Wagner MH (2009) Modelling elongational and shear rheology of two LDPE melts Rheol Acta 48: 691–697
16. Doi M, Edwards SFJ (1978) Dynamics of concentrated polymer systems. Part 2. Molecular motion under flow J. Chem Soc, Faraday Trans 74: 1802–1817

17. Doi M, Edwards SFJ (1979) Dynamics of concentrated polymer systems. Part 4. Rheological properties Chem Soc Faraday Trans 75: 38–54
18. Laun HM (1978) Description of the non-linear shear behaviour of a low density polyethylene melt by means of an experimentally determined strain dependent memory function Rheol Acta 17: 1–15
19. Rauschenberger V, Laun HM (1997) A recursive model for Rheotens tests J Rheol 41: 719–737
20. McLeish TCB, Larson RG (1998) Molecular constitutive equations for a class of branched polymers: The pom-pom polymers J Rheol 42: 81–110
21. Inkson NJ, McLeish TCB, Harlen OG, Groves DJ (1999) Molecular constitutive equations for a class of branched polymers: The pom-pom polymers J Rheol 43: 873–896
22. Likhtman AE, Graham RS (2003) Simple constitutive equation for linear polymer melts derived from molecular theory: Roli-poly equation J Non-Newtonian Fluid Mech 114: 1–12
23. Auhl D, Chambon P, McLeish TCB, Read DJ (2009) Elongational Flow of Blends of Long and Short Polymers: Effective Stretch Relaxation Time Phys Rev Lett 103:219801
24. van Ruymbeke, E Nielsen J, Hassager O (2010) Linear and nonlinear viscoelastic properties of bidisperse linear polymers: Mixing law and tube pressure effect J Rheol 54: 1155–1172
25. Borg T, Pääkkönen EJ (2009) Linear viscoelastic models: Part I. Relaxation modulus and melt calibration J Non-Newtonian Fluid Mech 156: 121–128
26. Borg T, Pääkkönen EJ (2009) Linear viscoelastic models: Part II. Recovery of the molecular weight distribution using viscosity data J Non-Newtonian Fluid Mech 156: 129–138
27. Borg T, Pääkkönen EJ (2009) Linear viscoelastic models: Part III. Start-up and transient flow effects from the molecular weight distribution J Non-Newtonian Fluid Mech 159: 17–25
28. Borg T, Pääkkönen EJ (2010) Linear viscoelastic models: Part IV. From molecular dynamics to temperature and viscoelastic relations using control theory J Non-Newtonian Fluid Mech 165: 24–31
29. Kurzbeck S, Oster F, Münstedt H (1999) Rheological properties of two polypropylenes with different molecular structure J Rheol 43: 359–374
30. Stadler FJ, Kaschta J, Münstedt H, Becker F, Buback M (2009) Influence of molar mass distribution and long-chain branching on strain hardening of low density polyethylene, Rheol Acta 48: 479–490
31. Rasmussen HK, Nielsen JK, Bach A, Hassager O (2005) Viscosity overshoot in the start-up of uniaxial elongation of low density polyethylene melts, J Rheol 49: 369–381
32. Burghelea TI, Starý Z, Münstedt H (2011) On the "viscosity maximum" during the uniaxial extension of a low density polyethylene J Non-Newtonian Fluid Mech 166: 1198–1209
33. Fleury G, Schlatter G, Muller R (2004) Non Linear Rheology for Long Chain Branching characterization, comparison of two methodologies: Fourier Transform Rheology and Relaxation Rheol Acta 44: 174–187

34. Malmberg A, Gabriel C, Steffl T, Münstedt H, Löfgren B (2002) Long-chain branching in metallocene-catalyzed polyethylenes investigated by low oscillatory shear and uniaxial extensional rheometry Macromolecules 35: 1038–1048
35. Costeux S (2003) Modeling of Randomly Branched Polymers Produced by Combination of Several Single-Site Catalysts: Toward Optimization of Melt Properties Macromolecules 36: 4168–4187
36. Chen X, Costeux C, Larson RG (2010) Characterization and prediction of long-chain branching in commercial polyethylenes by a combination of rheology and modeling methods J Rheol 54: 1185–1206
37. Wood-Adams PM, Dealy JM, deGroot AW, Redwine OD (2000) Effect of Molecular Structure on the Linear Viscoelastic Behavior of Polyethylene Macromolecules 33: 7489–7499
38. Sugimoto M, Suzuki Y, Hyun K, Ahn KH, Ushioda T, Nishioka A, Taniguchi T, Koyama K (2006) Melt rheology of long-chain-branched Polypropylenes Rheol Acta 46: 33–44
39. Vega JF, Expósito MT, Martínez-Salazar J, Lobón-Poo M, Barcina JO, Martínez AG, López M (2011) Molecular architecture and linear viscoelasticity of homogeneous ethylene/styrene copolymers Rheol Acta 50:207–220
40. Zimm BH, Stockmayer WH (1949) The dimensions of chain molecules containing branches and rings J Chem Phys 17:1301–1314
41. Vega JF, Fernándes M, Santamariá A, Muñoz-Escalona A, Lafuente P (1999) Rheological criteria to characterize metallocene catalyzed polyethylenes Macromol Chem Phys 200: 2257–2268
42. Gabriel C, Kokko E, Löfgren B, Seppälä J, Münstedt H (2002) Analytical and rheological characterization of long-chain branched metallocene-catalyzed ethylene homopolymers Polymer 43: 6383–6390
43. Malmberg A, Liimatta J, Lehtinen A, Löfgren B (1999) Characteristics of long chain branching in ethene polymerization with single site catalysts Macromolecules 32: 6687–6696
44. Malmberg A, Kokko E, Lehmus P, Löfgren B, Seppälä J (1998) Long-chain branched polyethene polymerized by metallocene catalysts Et[Ind]2ZrCl2/MAO and Et[IndH4]2ZrCl2/MAO Macromolecules 31: 8448–8454
45. Wood-Adams PM, Dealy JM (2000) Using rheological data to determine the branching level in metallocene polyethylenes Macromolecules 33: 7481–7488
46. Gabriel C, Münstedt H (2002) Influence of long-chain branches in polyethylenes on linear viscoelastic flow properties in shear Rheol Acta 41: 232–244
47. van Gurp M, Palmen J (1998) Time temperature superposition of polymeric blends Rheol Bull 67: 5–8
48. Trinkle S, Walter P, Friedrich C (2002) Van Gurp–Palmen Plot II—classification of long chain branched polymers by their topology Rheol Acta 41: 103–113
49. García-Franco CA, Srinivas S, Lohse DJ, Brant P (2001) Similarities between gelation and long chain branching viscoelastic behavior Macromolecules 34: 3115–3117

50. Keßner U, Kaschta J, Münstedt H (2009) Determination of method-invariant activation energies of long-chain branched low-density polyethylenes J Rheol 53: 1001–1016
51. Keßner U, Kaschta J, Stadler FJ, Le Duff CS, Drooghaag X, Münstedt H (2010) Thermorheological Behavior of Various Short- and Long-Chain Branched Polyethylenes and Their Correlations with the Molecular Structure, Macromolecules, 43: 7341–7350
52. Soares JBP, Hamielec AE Bivariate (1996) Chain Length and Long Chain Branching Distribution for Copolymerization of Olefins and Polyolefin Chains Containing Terminal Double Bonds Theory Simul 5: 547–572
53. Meimaroglou D, Krallis A, Saliakas V, Kiparissides C (2007) Macromolecules 40: 2224–2234
54. Meimaroglou D, Kiparissides C 2010 Macromolecules 43: 5820–5832
55. Costeux S, Wood-Adams P, Beigzadeh D (2002) Molecular Structure of Metallocene-Catalyzed Polyethylene: Rheologically Relevant Representation of Branching Architecture in Single Catalyst and Blended Systems Macromolecules 35: 2514–2528
56. Münstedt H, Kurzbeck S, Stange J (2006) Importance of Elongational Properties of Polymer Melts for Film Blowing and Thermoforming Polym Eng Sci 46: 1190–1195
57. Borg T (Muolon Oy) Method of producing a shrinkable product U.S. Patent 5,053,174, October 1 1991
58. Starý Z, Münstedt H (2008) Morphology Development in PS/LLDPE Blend During and After Elongational Deformation J Polym Sci Part B: Polym Phys 46: 16–27
59. Lohse DJ, Milner ST, Fetters LJ, Xenidou M, Hadjichristidis N, Menedelson RA, Garcia-Franco CA, Lyon MK (2002) Well-Defined, Model Long Chain Branched Polyethylene. 2. Melt Rheological Behavior, Macromolecules 35: 3066–3075